ENVIRONMENTAL RESEARCH
LETTERS

LETTER • OPEN ACCESS

Different trajectory patterns of ocean surface drifters modulated by near-inertial oscillations

To cite this article: Yuhang Zheng *et al* 2024 *Environ. Res. Lett.* **19** 104060

IOP Publishing Environ. Res. Lett. 19 (2024) 104060 https://doi.org/10.1088/1748-9326/ad7745

ENVIRONMENTAL RESEARCH
LETTERS

OPEN ACCESS

RECEIVED
25 July 2024

REVISED
20 August 2024

ACCEPTED FOR PUBLICATION
4 September 2024

PUBLISHED
12 September 2024

LETTER

Different trajectory patterns of ocean surface drifters modulated by near-inertial oscillations

Yuhang Zheng[1,2], Wei Wu[1], Minyang Wang[1], Yuhong Zhang[1] and Yan Du[1,2,*]

[1] Guangdong Key Laboratory of Ocean Remote Sensing, State Key Laboratory of Tropical Oceanography, South China Sea Institute of Oceanology, Chinese Academy of Sciences, Guangzhou, People's Republic of China
[2] University of Chinese Academy of Sciences, Beijing, People's Republic of China
* Author to whom any correspondence should be addressed.

E-mail: duyan@scsio.ac.cn

Keywords: near-inertial oscillations, drifter trajectories, near-inertial trajectory shape index, mesoscale eddy

Supplementary material for this article is available online

Abstract

Near-inertial oscillations (NIOs) are widely observed dynamic motions in the global ocean, with a frequency related to earth's rotation. Using a particle trajectory model, we found the combined influence of mesoscale eddies and NIOs could produce distinctive flower-like trajectories, which are a special case of near-inertial trajectories and were observed by surface drifters released within an anticyclone eddy in the South China Sea in 2021. The energy budget indicates that wind and geostrophic eddy currents are crucial in generating near-inertial energy during the flower-like trajectories. Furthermore, the particle trajectory model revealed variations in periods and widths of the near-inertial trajectory with latitudes. The width of near-inertial trajectories can exceed 8 km in the near-equatorial region and reach 3–6 km in the mid-latitude region (20°–50°). The ratios of near-inertial velocity to background velocity, defined as near-inertial trajectory shape index (NITSIs), lead to arc-shaped ($0.5 < \mathrm{NITSI} < 1.0$), overlapping semi-circular ($\mathrm{NITSI} > 1.0$), and near-circular trajectories ($\mathrm{NITSI} \gg 1.0$). Globally, approximately 1/3 of the drifters' lifespan featured clear near-inertial trajectories, with a significant presence in most middle latitudes and the largest NITSI in the north Pacific westerly. These findings highlight the importance of NIOs and suggest their substantial impact on local surface matter distribution, trajectory prediction, and marine rescue operations.

1. Introduction

Near-inertial oscillations (NIOs) are commonplace motions in the global ocean with a frequency near the inertial frequency (Pollard and Millard 1970, D'Asaro 1985). Near-inertial kinetic energy constitutes a significant portion of the upper ocean's kinetic energy (Thomson *et al* 1998). Wind forcing is the primary mechanism for generating NIOs, as it transfers momentum into the surface mixed layer (Pollard 1970, Price 1981, Chen *et al* 2013). In addition to the energy input from wind, the near-inertial energy of the mixed layer may also be attributed to the energy transfer associated with the geostrophic flow (Jing *et al* 2017, Barkan *et al* 2021). The energy transfer efficiency could be represented by the ratio of the eddy-to-NIO energy transfer rate (ε) to the near-inertial wind work (W), ε/W. Previous studies suggest it is relatively low (~1%) (e.g. Jing *et al* 2017). Recently, Liu *et al* (2023) utilized a Satellite-tracked surface drifter data set from the Global Drifter Program (GDP) (Elipot *et al* 2016) and derived a global integral of ε, reaching 0.025 TW ($1\mathrm{TW} = 10^{12}\mathrm{W}$). Considering a global W integral value of 0.2–0.6 TW (Furuichi *et al* 2008, Liu *et al* 2019, Alford 2003, 2020, Liu *et al* 2023), the energy transfer efficiency is 4%–13%, indicating a significant contribution of eddies to NIOs.

In recent years, surface drifter data have been widely used in oceanographic analyses (Lumpkin and Johnson 2013, Qian *et al* 2013, Essink *et al* 2019, Arbic *et al* 2022, Wang *et al* 2022, Zhao *et al* 2023). Understanding the movement characteristics of drifters holds significant importance for marine surface

material transport, oil spill tracking, and maritime search and rescue operations (Lumpkin *et al* 2017). Drifter data from GDP provide nearly global coverage of drifter positions and horizontal current velocities at hourly intervals (Elipot *et al* 2016), facilitating the study of NIOs on a global scale. Numerous studies have revealed the characteristics of NIOs using drifter data (Park *et al* 2005, Chaigneau *et al* 2008, Liu *et al* 2019, Liu *et al* 2023, Arbic *et al* 2022). Under ideal conditions, NIOs manifest as circular motion of water particles, with the Coriolis force acting as centripetal force. In the real ocean, the near-inertial trajectories of drifters are commonly observed as anticyclone loops, which are prevalent worldwide. Interestingly, NIOs can result in different trajectory patterns for surface drifters across time and regions. In certain regions, such as the northeast Pacific, trajectories sometimes closely adhere to near-circular paths (Thomson *et al* 1998, Alford *et al* 2016), while in other cases they may appear as semi-circular or arc-shaped paths (Assireu *et al* 2017, Crawford *et al* 1998, Essink *et al* 2019, Poulain 1990, Röhrs *et al* 2023). Nevertheless, there has been a lack of exploration of the underlying causes of the varying near-inertial trajectories exhibited by surface drifters in the existing literature.

In 2021, distinctive flower-like trajectories were observed in the surface drifters released within a long-lived anticyclone eddy in the South China Sea (SCS). This work aims to figure out the underlying causes of these flower-like trajectories. The structure of the paper is as follows: section 2 describes the methodology and data. In section 3, a simple Lagrangian model is developed to elucidate the factors contributing to distinct near-inertial trajectories, including those exhibiting flower-like patterns. Then, we provide the global distribution of these distinct near-inertial trajectories. Section 4 discusses the potential practical implications of these near-inertial trajectories, followed by the concluding remarks.

2. Data and methodology

2.1. Data

Two drifter datasets are used in this study. The first dataset comprises 30 surface drifters deployed in 2021 by the South China Sea Institute of Oceanology, Chinese Academy of Sciences. These 30 drifters tracked by Global Positioning System (GPS) were deployed in two batches within the northern SCS domain (112°–116° E, 16°–19° N) in May and September 2021. They adhere to the same design as the Atlantic Oceanographic and Meteorological Laboratory (AOML) drifters and consist of a surface float and a drogue intended to minimize slip caused by wind and waves (Niiler and Paduan 1995). The float remains at the sea surface and transmits the drifter's location (with an accuracy of about 10 m) at 35 min intervals to the GPS satellites. To facilitate analysis, this drifter dataset is interpolated into hourly intervals using the Kriging interpolation method (Hansen and Poulain 1996).

The second dataset consists of historical drifters from the GDP, providing hourly velocity and location estimates (Elipot *et al* 2016), which is maintained by the AOML. The drifters are equipped with a drogue at a depth of 15 m. Loss of the drogue, known as undrogued drifters, can introduce significant observation bias due to wind drag on the surface float (Laurindo *et al* 2017). The GDP data used in this study is version 2.01, spanning from 1987 to 2022 and containing 19 396 individual surface drifter trajectories. Trajectories with more than 10 consecutive missing values are divided into two sub-trajectories; otherwise, missing values are linearly interpolated. Subsequently, sub-trajectories that are less than 300 h in duration are excluded. Following data processing, 37 255 sub-trajectories were obtained. To mitigate the influence of wind slippage, wind data from the European Centre for Medium-Range Weather Forecasts Reanalysis V5 (Hersbach *et al* 2020), which is of hourly temporal and 0.25° spatial resolutions, are employed for drifter velocity correction (Pazan and Niiler 2001):

$$\vec{\boldsymbol{u}} = \vec{\boldsymbol{u}}_{\boldsymbol{dr}} - \boldsymbol{k}\vec{\boldsymbol{u}}_{\boldsymbol{w}} \tag{1}$$

where $\vec{\boldsymbol{u}}_{\boldsymbol{dr}}$ is the drifter velocity, $\vec{\boldsymbol{u}}_{\boldsymbol{w}}$ is the wind velocity linearly interpolated to the position and time of drifter observations, and $\boldsymbol{k}$ is the coefficient of correction. When the drifter is drogued, the coefficient is $\boldsymbol{k_d} = 7 \times 10^{-4}$ (Niiler and Paduan 1995, Pazan and Niiler 2001). When the drifter is undrogued, the coefficient applied is (Laurindo *et al* 2017):

$$\boldsymbol{k_u} = \left(\overline{\boldsymbol{u}}_{\boldsymbol{u}} - \overline{\boldsymbol{u}}_{\boldsymbol{d}}\right)/\overline{\boldsymbol{u}}_{\boldsymbol{w}} + \boldsymbol{k_d} \tag{2}$$

where $\overline{\boldsymbol{u}}_{\boldsymbol{d}}$ and $\overline{\boldsymbol{u}}_{\boldsymbol{u}}$ represent the downwind components of the drogued and undrogued drifter velocities, respectively, $\overline{\boldsymbol{u}}_{\boldsymbol{w}}$ is the amplitude of wind speed, and the upper horizontal bar denotes spatially averaged value in a 2° × 2° spatial box. Atmospheric forcing (10 m wind speed) data from the National Centers for Environmental Prediction Climate Forecast System Version 2 (CFSv2, Saha *et al* 2014) hourly product is also utilized for wind work calculations.

Daily sea level anomaly (SLA) is derived from Copernicus Marine environment monitoring service with a 1/4° × 1/4° spatial resolution to depict the location and intensity of the eddy throughout the drifters' lifespan.

2.2. Construction of a Lagrangian trajectory model

First, we decompose the total velocity $\vec{\boldsymbol{u}}_{\boldsymbol{a}}$ in the upper ocean into near-inertial velocity $\vec{\boldsymbol{u}}_{\mathbf{in}}$ and background

velocity $\vec{u}_b$, All other types of flow except near-inertial flow are included in the background velocity,

$$\vec{u}_a = \vec{u}_{\mathrm{in}} + \vec{u}_b. \tag{3}$$

For near-inertial motion, in an idealized state neglecting energy input and dissipation, it can be expressed by equation (4), where (u_{in}, v_{in}) denote the zonal and meridional near-inertial velocity, and f represents the Coriolis frequency ($f = 2\omega\sin\varphi$, where φ is the latitude, $\omega = 7.29 \times 10^{-5}\mathrm{rad\ s^{-1}}$),

$$\begin{cases} \frac{\partial u_{\mathrm{in}}}{\partial t} - f v_{\mathrm{in}} = 0 \\ \frac{\partial v_{\mathrm{in}}}{\partial t} + f u_{\mathrm{in}} = 0 \end{cases} \tag{4}$$

The trajectory of the particle, as governed by equations (3) and (4), is characterized by three independent variables: background velocity $\vec{u}_b$, near-inertial velocity $\vec{u}_{\mathrm{in}}$ and the Coriolis frequency f. This study adopts the variable-controlling approach to investigate the influence of each variable on the particle trajectory. The Eulerian method (Spydell and Feddersen 2009, Wu *et al* 2022) simulates the Lagrangian trajectory under a constant uniform background velocity:

$$\vec{L}_2 = \vec{L}_1 + \vec{u}_{a1} \cdot (t_2 - t_1) \tag{5}$$

where $\vec{u}_{a1}$ is the velocity at t_1, $\vec{L}_1$ and $\vec{L}_2$ are the locations at t_1 and t_2. A time interval of 1 s is used in the simulation to prevent significant decay of the near-inertial velocity. Furthermore, to investigate the drifter trajectory within the eddy, a constant eddy background flow field is established to simulate the Lagrange trajectory. The eddy background flow field rotates clockwise with a fixed rotational angular velocity $\vec{\omega}$. Therefore, the background velocity is $\vec{u}_b = \vec{\omega} \times \vec{l}$, where $\vec{l}$ represents the position vector of the particle. A damping term r is incorporated as described in equation (6) to replicate real ocean conditions better. This term accounts for the decay of mixed layer motions resulting from wave propagation. The average value of r in the global ocean is approximately $0.15\,f$ (Alford 2001, 2003),

$$\begin{cases} \frac{\partial u_{\mathrm{in}}}{\partial t} + r u_{\mathrm{in}} - f v_{\mathrm{in}} = 0 \\ \frac{\partial v_{\mathrm{in}}}{\partial t} + r v_{\mathrm{in}} + f u_{\mathrm{in}} = 0 \end{cases} \tag{6}$$

It is crucial to emphasize that the near-inertial velocity is specified at the initial moment in our simulation. In real ocean scenarios, input for near-inertial velocity includes wind work and geostrophic energy transfer (Jing *et al* 2017). Assuming that the near-inertial and geostrophic flows are vertically uniform in the surface boundary layer, we can obtain,

$$\begin{cases} \frac{\partial u_{\mathrm{in}}}{\partial t} + u_{\mathrm{in}} U_x + v_{\mathrm{in}} U_y + r u_{\mathrm{in}} - f v_{\mathrm{in}} = \frac{\tau_x}{\rho_0 H_M} \\ \frac{\partial v_{\mathrm{in}}}{\partial t} + u_{\mathrm{in}} V_x + v_{\mathrm{in}} V_y + r v_{\mathrm{in}} + f u_{\mathrm{in}} = \frac{\tau_y}{\rho_0 H_M} \end{cases} \tag{7}$$

where (U, V) is the geostrophic flow, which is horizontally nondivergent; H_M is the climatological monthly mean mixed layer depth from World Ocean Atlas (WOA2018); (τ_x, τ_y) is the wind stress, which is normalized by the product of seawater density ρ_0 and mixed layer depth H_M.

2.3. Energy budget

Due to the large change of inertial frequency along long drifter trajectories, velocity estimates tracked by a drifter are divided into half-overlapping 300-hour segments in order to extract the near-inertial velocities $\vec{u}_{\mathrm{in}}$ (Liu *et al* 2023, 2019). The near-inertial band 0.75 f–1.25 f is adopted, where f is the mean Coriolis frequency of each segment. The near-inertial kinetic energy (NIKE) is then calculated as,

$$KE = \rho_0 H_M \left({u_{\mathrm{in}}}^2 + {v_{\mathrm{in}}}^2 \right) / 2. \tag{8}$$

The diagnostic equation of NIKE can be deduced from equations (7) and (8),

$$\frac{\partial KE}{\partial t} = \varepsilon - 2rKE + W \tag{9}$$

where W is near-inertial wind work, ε represents the eddy-to-NIO energy transfer rate.

The near-inertial wind work is,

$$W = \vec{\tau} \cdot \vec{u}_{\mathrm{in}} \tag{10}$$

where $\vec{\tau}$ is the wind stress vector calculated as (Alford 2020, Liu *et al* 2019),

$$\vec{\tau} = \rho_a C_D \left| \vec{U}_{10} - \vec{u} \right| \left(\vec{U}_{10} - \vec{u} \right) \tag{11}$$

where $\rho_a = 1.3\ \mathrm{kg\ m^{-3}}$ is the air density, C_D is the drag coefficient following the definition in (Oey *et al* 2006), and $\vec{U}_{10}$ is the 10 m wind velocity vector,

$$C_D \times 10^{-3} = \begin{cases} 1.2, & \left| \vec{U}_{10} \right| \leqslant 11\,m/s \\ 0.49 + 0.065 \left| \vec{U}_{10} \right|, & 11 < \left| \vec{U}_{10} \right| \leqslant 19\,m/s \\ 1.364 + 0.0234 \left| \vec{U}_{10} \right| - 0.0002 \left| \vec{U}_{10} \right|^2, & \\ 19 < \left| \vec{U}_{10} \right| \leqslant 100\,m/s & \end{cases} \tag{12}$$

The energy transfer rate is,

$$\begin{aligned} \varepsilon = -\rho_0 H_M (& u_{\mathrm{in}} u_{\mathrm{in}} U_x + u_{\mathrm{in}} v_{\mathrm{in}} U_y \\ & + u_{\mathrm{in}} v_{\mathrm{in}} V_x + v_{\mathrm{in}} v_{\mathrm{in}} V_y). \end{aligned} \tag{13}$$

The geostrophic velocity $\boldsymbol{U}$ is obtained by low-pass filtering $\vec{u} - \vec{u}_m$ (where $\vec{u}_m$ is the climatological mean of $\vec{u}$) with a cutoff period of 7 d, and the gradient of the geostrophic current is calculated from data at two consecutive locations of drifters (Zhang and Qiu 2018, Liu *et al* 2023).

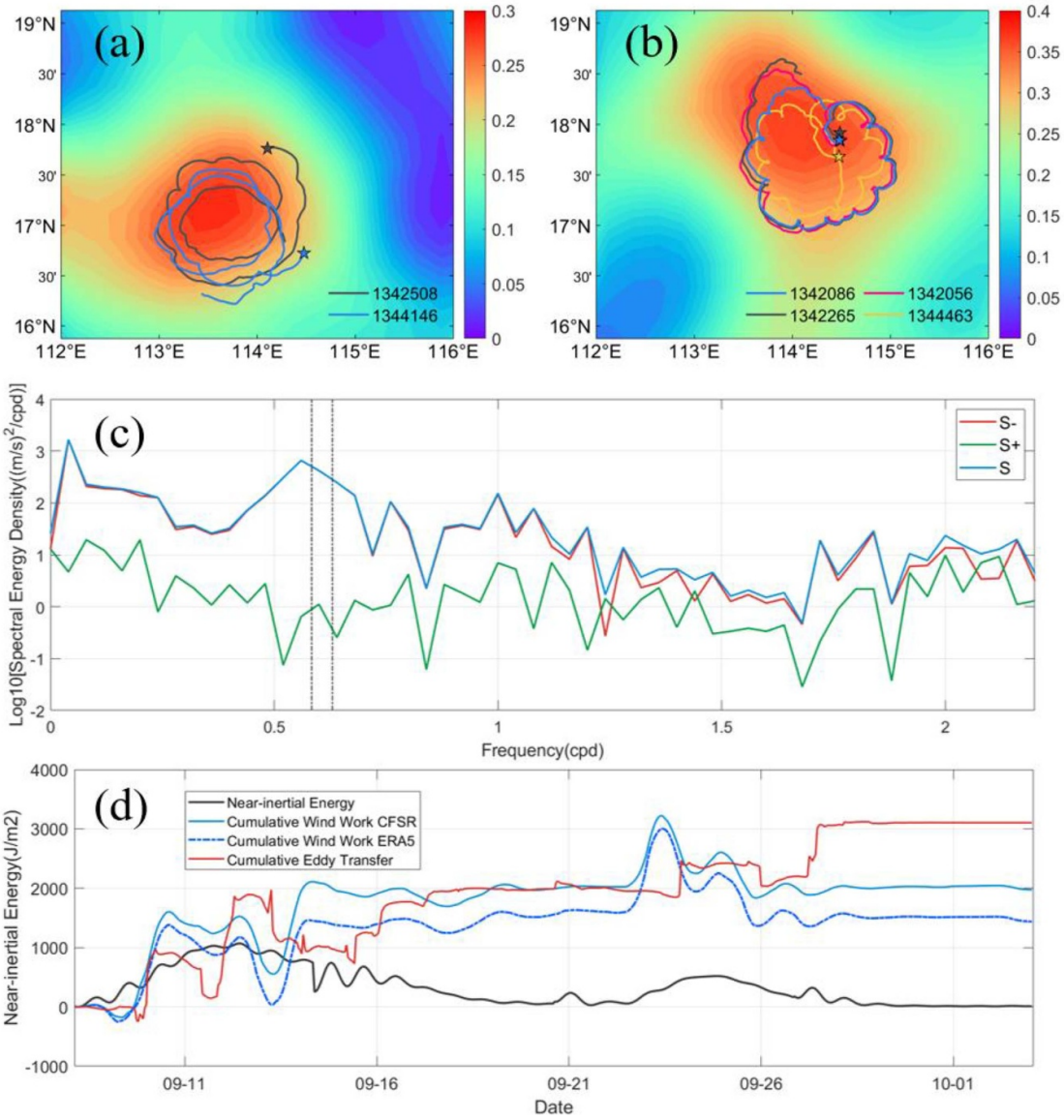

Figure 1. (a) Trajectories of drifters deployed in the South China Sea in 2021 from 27 May to 21 June. The grey and blue lines represent the trajectories of drifters (Nos. 1342508 and 1344146). Stars denote the deployment locations. The shaded areas represent Sea Level anomalies (SLA, units: m) in meters on June 10. (b) Similar to (a), but with trajectories from 8 September to 3 October and the SLA on September 20. The blue, red, grey, and yellow lines represent trajectories of drifters (Nos. 1342086, 1342056, 1342265 and 1344463). (c) Rotary spectra of the drifter (No. 1342086). The red, green, and blue lines represent the clockwise, counterclockwise, and total spectra, respectively. The black dotted line represents the local inertial frequency range. (d) Energy budget of the drifter NO.1342086. The black lines represent the near-inertial energy. The red and blue lines represent the cumulative energy transfer from the initial moment of mesoscale eddy and wind work, respectively. The light blue solid line is calculated using CFSv2 data, while the dark blue dashed line uses ERA5 data.

3. Results

3.1. Observed flower-like trajectories

Remarkable flower-like trajectories were observed in surface drifters released within an anticyclonic eddy in the northern SCS during May (figure 1(a)) and September (figure 1(b)) 2021. Based on previous observations, these anticyclonic arcs are probably linked to NIOs. Taking drifter No. 1342086 (blue line in figure 1(b)) as an example, the rotary spectra (figure 1(c)) show that the clockwise spectral energy density is significantly larger than the counterclockwise one in nearly all frequency bands. Both the clockwise and total spectral energy densities exhibit a distinct peak slightly below the local inertial frequency, a characteristic feature of NIOs. The frequency shift of the inertial frequency may be attributed to the influence of background vorticity ξ (Kunze 1985), following equation (14),

$$f_{\text{eff}} = f + \xi/2 \tag{14}$$

Since ξ is negative in the anticyclone eddy, the effective Coriolis frequency f_{eff} is slightly lower than

the local Coriolis frequency f. Furthermore, the near-inertial energy exhibits a prominent bimodal structure, peaking on 13 and 24 September, respectively (figure 1(d)). The maximum near-inertial energy recorded reaches 1000 J m^{-2}, indicating a strong presence of NIOs within the observing period.

3.2. Causes of different near-inertial trajectories

In addition to these flower-like trajectories, drifters characterized by NIOs also exhibit other trajectory patterns. We refer to them as near-inertial trajectories. To investigate the causes of these different near-inertial trajectories, we developed a Lagrangian trajectory model and presented the simulated trajectories. Figures 2(a) and (b) depict particle simulations conducted under a constant uniform background flow field (northeastward), with particles released from the origin. Figures 2(c)–(f) illustrate simulations under a constant eddy background flow field, with particles released north of the eddy center (the origin) at a distance of half the radius of the eddy. Further experimental details are provided in table 1. We used diverse experimental data for testing and obtained consistent results. Therefore, the provided experimental details are sufficient for the considerations required by this study. Figure 2(a) demonstrates an interesting phenomenon, specifically the significant variation in particle trajectory observed at different ratios of near-inertial velocity to background velocity, which is defined as a near-inertial trajectory shape index (NITSI), representing the shape of the near-inertial trajectory of particles. When the background velocity equals 0 (NITSI equals infinity), the particle trajectory forms a complete circle with a radius of u_{in}/f as calculated by equation (4). When NITSI is much greater than 1 (e.g. NITSI = 5), the trajectory exhibits a near-circular shape. When NITSI is slightly greater than 1, the trajectory exhibits an overlapping semi-circular shape. When NITSI is between 0–1, the trajectory takes on an arc shape. Notably, when NITSI equals exactly 1, the trajectories from the adjacent two periods of near-inertial motion do not intersect. These findings allow for a visual approximation of the ratio of near-inertial velocity to background velocity by observing the drifter trajectory. In addition to near-inertial velocity and background velocity, latitude affects near-inertial trajectories. The differing latitudes result in different inertial frequencies, leading to noticeable variations in trajectory periods and widths. Specifically, the trajectories in the lower/higher latitude region exhibit longer/shorter periods and wider/narrower widths (figure 2(b)). Additionally, the near-inertial trajectory widths (NITW) of all trajectories equal $|2u_{in}/f|$, implying that NITW decreases with the latitude and increases with the near-inertial velocity. NITW has the potential to extend the reach of background flow influence and could impact the distribution of surface matter in the ocean.

Surprisingly, when an eddy dominates the background flow, these particles exhibit flower-like trajectories similar to those observed in the SCS (figure 2(c)). While the shapes of the three trajectories are comparable, their widths differ. The near-inertial flow rates can be likened to adjusting the size of petals in a flower, with higher near-inertial flow rates resulting in larger petals. In the eddy, it is evident that eddy velocities could change the near-inertial trajectories. The three trajectories maintained consistent widths but covered varying distances (figure 2(d)). The eddy velocity (eddy radius) can be perceived as modifying the number of petals in a flower, where greater eddy velocities (shorter eddy radius) correspond to an increased number of petals. The latitude affects the near-inertial trajectory inside an eddy and can be likened to influencing the size and number of petals in a flower (figure 2(e)). The blue trajectory in figure 2(e) simulates the observed drifter No.1342086, recording a near-inertial velocity of 0.18 m s^{-1}, an eddy velocity of 0.28 m s^{-1}, and an eddy radius of 70 km on average. The simulated results closely align with the drifter trajectory, confirming the model's validity and precision.

The above simulations do not consider the decay of the near-inertial energy ($r = 0$), which is not negligible in the actual ocean. When $r = 0.02f$, the near-inertial energy dissipates slowly, resulting in a relatively distinct near-inertial trajectory during one rotation within the eddy (figure 2(f)). Conversely, when $r = 0.05\,f$ (or $0.15\,f$), the near-inertial trajectory nearly disappears after 3 (or 1) inertial period. Alford (2003) proposed that r is approximately equal to $0.15\,f$ in actual ocean conditions, suggesting that without sustained energy input, the drifter would not exhibit the observed flower-like trajectory. Based on this, an energy budget analysis was conducted for drifter No. 1342086 (figure 1(d)). The near-inertial energy exhibits a clear bimodal structure, and these two peaks lead the drifter to experience elevated near-inertial energy during one rotation following the eddy, resulting in a flower-like trajectory. During the first peak (8–20 September), both the wind and the geostrophic eddy current contributed more than 1000 J m^{-2} of energy into the near-inertial current. Calculating wind work based on ERA5 and CFSR data, the ratios of ε/W were 1.3 and 1.0, respectively. These ratios are one order of magnitude larger than the global average (Liu *et al* 2023). The geostrophic current performed positive work during the second peak (22–28 September). Even though the wind work yielded negative values throughout the second peak, the positive work of the wind played a crucial role in the initial increase of near-inertial energy. The calculations are similar for several other drifters (figure

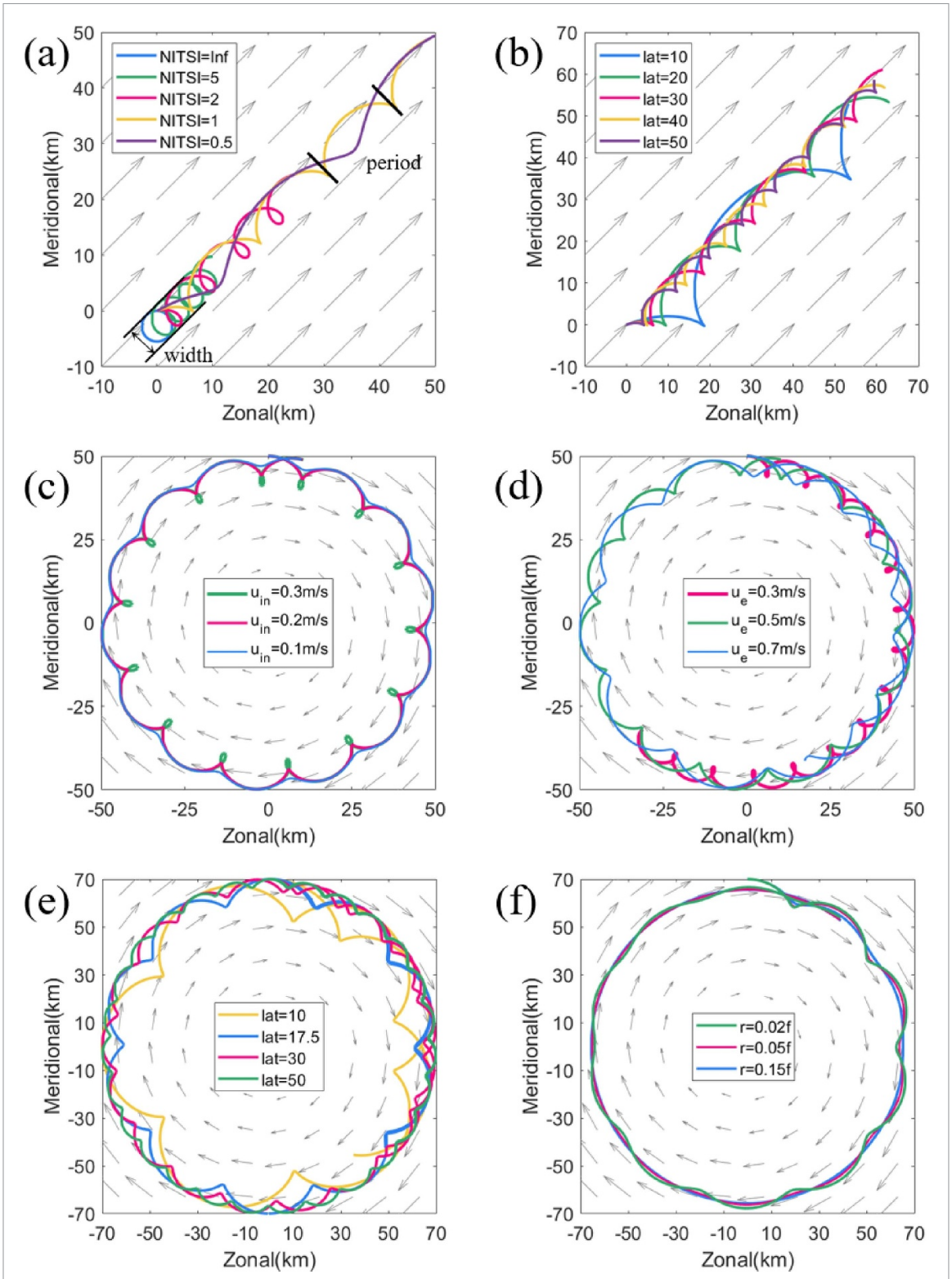

Figure 2. Trajectories simulated by the variable-controlling method with the Lagrangian trajectory model. Grey arrows indicate the direction and relative velocity of the background flow. (a) The blue, green, pink, yellow, and purple lines represent scenarios where NITSI equals infinity, 5, 2, 1, and 0.5, respectively. Black arrows indicate near-inertial trajectory width. The time of the yellow trajectory between the two black lines is one period. (b) The blue, green, pink, yellow, and purple lines represent scenarios where the drifter is located at latitudes of 10°N, 20°N, 30°N, 40°N and 50°N. (c) The green, pink, and blue lines represent scenarios where the near-inertial velocity equals 0.3, 0.2 and 0.1 m s^{-1}. (d) The pink, blue, and green lines represent scenarios where the eddy edge velocity u_e ($\omega \cdot ra$) equals 0.3, 0.5 and 0.7 m s^{-1}. (e) The yellow, blue, pink, and green lines represent scenarios where the drifter is located at latitudes of 10°N, 17.5°N, 30°N and 50°N. (f) The green, pink, and blue lines represent scenarios where the dissipation coefficient r is 0.02, 0.05, and 0.15 times the local Coriolis frequency f. Further experimental details are provided in table 1.

Table 1. The conditions set in each subgraph of figure 2. All simulations are confined to the Northern Hemisphere. The initial zonal near-inertial velocity is denoted by u_{in0} and the initial meridional v_{in0} is set to 0. The constant background velocity is expressed as u_b and r represents the damping term in equation (6). The radius and angular velocity of background eddy field are denoted by ra and ω, respectively.

	Latitude (°N)	u_{in0} (m s^{-1})	u_b (m s^{-1})	ra (km)	ω·ra (m s^{-1})	r
a	30	0.2	variable	/	/	0
b	variable	0.2	0.2	/	/	0
c	30	variable	/	100	0.5	0
d	30	0.2	/	100	variable	0
e	variable	0.18	/	140	0.56	0
f	17.5	0.18	/	140	0.56	variable

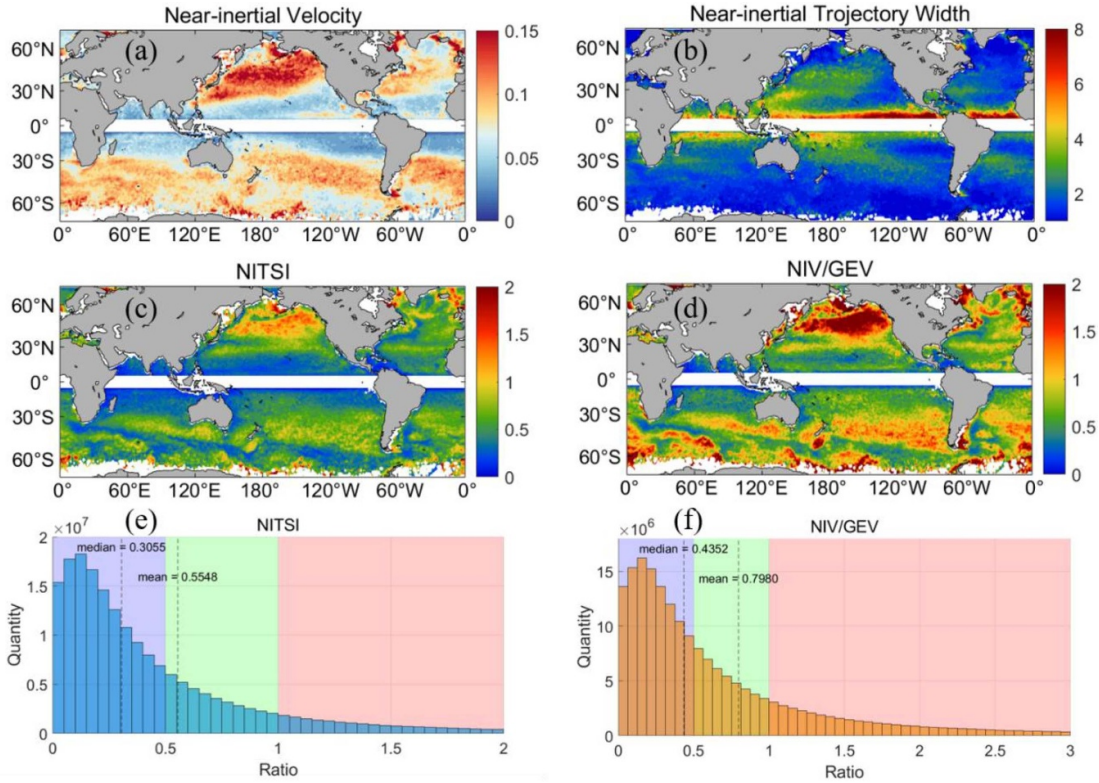

Figure 3. Climatological means of (a) near-inertial velocity (units: m s^{-1}) and (b) near-inertial trajectory width (units: km). Spatial distribution of (c) NITSI (ratio of near-inertial velocity to background velocity) and (d) NIV/GEV (ratio of near-inertial velocity to geostrophic eddy velocity). (e) Histogram of NITSI. The blue shaded area refers to inapparent arc-shaped trajectories. The green shaded area refers to significant arc-shaped trajectories, while the red shaded area refers to semi-circle and near-circular trajectories (The NITSI $>$ 2 part is not shown). Blue, green, and red areas accounted for 67.4%, 18.7%, and 13.9% of the data, respectively. (f) Histogram of NIV/GEV. Blue, green, and red areas accounted for 54.9%, 22.2%, and 22.9% of the data, respectively.

not shown), so it is evident that both wind and geostrophic eddy current play a crucial role in generating the near-inertial energy during the flower-like trajectories.

3.3. Global distribution of near-inertial trajectories

To further investigate this issue, GDP data was utilized to calculate the worldwide distribution of near-inertial velocity (figure 3(a)) and NITW (figure 3(b)). Near-inertial velocities are generally higher in westerly wind regions and lower in low latitudes. The North Pacific is the most significant region featured with near-inertial velocities, approximately 0.15 m s^{-1} on average. NITW increases with the decrease of latitude on the whole, and it can reach more than 8 km in the near-equatorial region and 3–6 km in regions characterized by large values of near-inertial velocity within mid-latitude region (20°–50°). Globally, the highest NITSI reaches 1.5 or higher in the northeast Pacific and exceeds 0.5 in other westerly, indicating significant arc-shaped near-inertial trajectories (figure 3(c)). The median and average of the NITSI are 0.31 and 0.56 (figure 3(e)). NITSI exceeds 0.5 (1.0) in 32.6% (13.9%) drifter lifespans. The global distribution of the ratio of near-inertial velocity to geostrophic eddy velocity (NIV/GEV) shows results similar to those of NITSI (figure 3(d)). NIV/GEV exceeds 0.5 (1.0) in 45.1% (22.9%) drifter

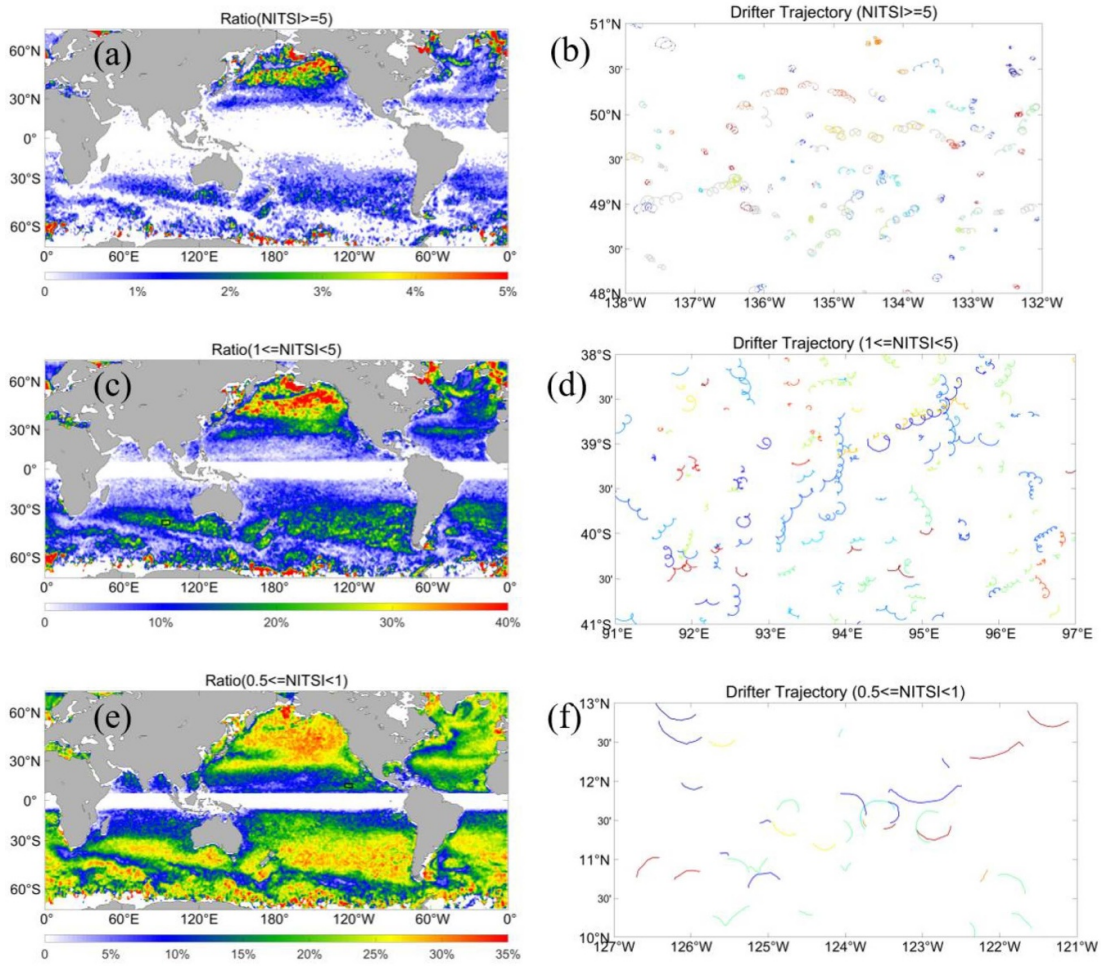

Figure 4. Global distribution of proportion with (a) NITSI >5, (c) $1 \leqslant$ NITSI <5, and (e) $0.5 \leqslant$NITSI <1. Detailed real drifter trajectories within the black rectangular area in (a), (c) and (e) are shown in (b), (d) and (f). All trajectories shown persist for more than 24 h. Different colors indicate different drifter trajectories. Panel (b) specifically displays trajectories with $2 \leqslant$ NITSI <5 in grey for clarity and the trajectories of NITSI $\geqslant 5$ are represented in multiple colors.

lifespans (figure 3(f)). Despite the eddy kinetic energy being significantly larger than the near-inertial energy (Ferrari and Wunsch 2009), near-inertial velocities surpass the geostrophic eddy velocity in nearly a quarter of drifter lifespans. This highlights the significance of NIOs in ocean surface dynamics and their potential impact on local Lagrangian transports.

To validate those findings, we also generated global maps illustrating the distribution of various NITSI proportions and actual drifter trajectories in representative regions. The Northeast Pacific Ocean exhibits the highest proportion of NITSI >5 drifters, reaching up to 5% (figure 4(a)), which explains why near-circular trajectories are often observed in this area (figure 4(b)) and less so in other areas. For NITSI values between 1 and 5, the Northeast Pacific Ocean again demonstrates the largest proportion, reaching approximately 40% (figure 4(c)), while other westerlies can account for up to 20%. Real drifter trajectories in these areas exhibit semi-circular patterns consistent with our previous results (figure 4(d)). When considering NITSI values between 0.5 and 1, most mid-latitude regions show proportions exceeding 25%, with relatively lower proportions observed in strong current regions at around 10% (figure 4(e)). Corresponding real drifter trajectories in near-equatorial regions reveal a significant arc shape, with significantly greater width compared to high latitude regions (figure 4(f)). These real drifter trajectories across different regions corroborate the conclusions drawn from our Lagrangian model analysis.

4. Summary and discussion

Previous studies have indicated that near-inertial turbulence mixing, induced by NIOs and downward-propagating near-inertial waves (NIWs), can facilitate the exchange of nutrient fluxes between the deep layer and the upper ocean, resulting in alterations in chlorophyll concentration and phytoplankton abundance (Granata *et al* 1995, Zhang *et al* 2014, Wang *et al* 2020). Besides, NIOs are essential in the

horizontal distribution of local surface matter and trajectory prediction. Our particle trajectory simulations based on HYCOM reanalysis data indicate these two points. With or without near-inertial velocity, the simulated local particle concentration differs significantly (supplementary figure S1). After removing the near-inertial velocity, except that the arc trajectories of particles are no longer obvious, the motion direction of some particles has a significant deviation from the original a few days later (supplementary figure S2).

By constructing a Lagrangian model, we examined the variation of near-inertial trajectories at different near-inertial velocities, latitudes, and background velocities in both a constant horizontal flow field and an eddy field. We elucidated that the flower-like trajectories observed in the SCS are attributed to mesoscale eddy and NIOs, through which wind and geostrophic eddy currents contribute energy to NIOs. Using this model, we also found different latitudes, which determine the inertial frequencies, leading to noticeable variations in trajectory periods and widths. NITW can reach more than 8 km in the near-equatorial region and 3–6 km in areas characterized by high values of near-inertial velocity within westerly wind regimes, potentially expanding the influence range of low-frequency flow. The ratios of near-inertial velocity to background velocity, defined as NITSIs, result in arc-shaped, overlapping semi-circular, and near-circular trajectories of drifters. $0.5 < \text{NITSI} < 1.0$ indicates significant arc-shaped trajectories. $\text{NITSI} > 1.0$ indicates overlapping semi-circular shapes, and $\text{NITSI} \gg 1.0$ indicates near-circular shapes. Globally, approximately 1/3 of the drifters' lifespan featured clear near-inertial trajectories, with a significant presence in most middle latitudes and the largest NITSI in the north Pacific westerly. These findings highlight the importance of NIOs in the upper ocean and suggest that NIOs may have substantial implications for local surface matter distribution, trajectory prediction, and marine rescue operations.

Data availability statement

Data sets of drifters deployed in 2021 cruise for this manuscript are available at the National Earth System Science Data Center (www.geodata.cn/main/face_science_detail?typeName=face_science&guid=39099061696594). GDP drifter data are provided by AMOL, available at www.aoml.noaa.gov/phod/gdp/hourly_data.php. SLA data are obtained from CMEMS website (https://data.marine.copernicus.eu/product/SEALEVEL_GLO_PHY_L4_MY_008_047/services). ERA5 wind data is provided by ECMWF, downloaded from https://cds.climate.copernicus.eu/cdsapp#!/dataset/reanalysis-era5-single-levels?tab=form. CSFv2 wind data and HYCOM data are obtained from the U. S. Global Ocean Data Assimilation Experiment website www.hycom.org/dataserver/ncep-cfsv2 and www.hycom.org/dataserver/gofs-3pt1/analysis. The WOA2018 climatological monthly mean mixed layer depth data are available at www.ncei.noaa.gov/access/world-ocean-atlas-2018/bin/woa18.pl.

All data that support the findings of this study are included within the article (and any supplementary files).

Acknowledgment

Data were collected on board R/V Shiyan-6 and R/V Shiyan-1 implementing the open research cruise NORC2021-302 supported by NSFC fund and NSFC Ship-time Sharing Project (42090042, 42430401, 42049907, and 41976024). We thank the crew for their help during the cruise. We also thank the data archive support from the National Earth System Science Data Center, National Science & Technology Infrastructure of China (www.geodata.cn). This study is supported by the Southern Marine Science and Engineering Guangdong Laboratory (Guangzhou) (2019BT02H594), the Chinese Academy of Sciences (XDB42010305, 133244KYSB20190031, SCSIO202201, and SCSIO202204), and the Open Project Program of State Key Laboratory of Tropical Oceanography (LTOZZ2101, LTOZZ2203).

ORCID iD

Yan Du https://orcid.org/0000-0002-7842-0801

References

Alford M H 2001 Internal swell generation: the spatial distribution of energy flux from the wind to mixed layer near-inertial motions *J. Phys. Oceanogr.* **31** 2359–68

Alford M H 2003 Improved global maps and 54-year history of wind-work on ocean inertial motions *Geophys. Res. Lett.* **30** 1424

Alford M H 2020 Revisiting near-inertial wind work: slab models, relative stress, and mixed layer deepening *J. Phys. Oceanogr.* **50** 3141–56

Alford M H, MacKinnon J A, Simmons H L and Nash J D 2016 Near-inertial internal gravity waves in the ocean *Annu. Rev. Mar. Sci.* **8** 95–123

Arbic B K *et al* 2022 Near-surface oceanic kinetic energy distributions from drifter observations and numerical models *J. Geophys. Res.: Oceans* **127** e2022JC018551

Assireu A T, Dauhut T, Dos Santos F A and Lorenzzetti J A 2017 Near-inertial motions in the Brazil Current at 24°S–36°S: observations by satellite tracked drifters *Contrib. Shelf Res.* **145** 1–12

Barkan R, Srinivasan K, Yang L, McWilliams J C, Gula J and Vic C 2021 Oceanic mesoscale eddy depletion catalyzed by internal waves *Geophys. Res. Lett.* **48** e2021GL094376

Chaigneau A, Pizarro O and Rojas W 2008 Global climatology of near-inertial current characteristics from Lagrangian observations *Geophys. Res. Lett.* **35** L13603

Chen G, Xue H, Wang D and Xie Q 2013 Observed near-inertial kinetic energy in the northwestern South China Sea *J. Geophys. Res.: Oceans* **118** 4965–77

Crawford W R, Cherniawsky J Y and Foreman M G G 1998 Rotary velocity spectra from short drifter tracks *J. Atmos. Ocean. Technol.* **15** 731–40

D'Asaro E A 1985 The energy flux from the wind to near-inertial motions in the surface mixed layer *J. Phys. Oceanogr.* **15** 1043–59

Elipot S, Lumpkin R, Perez R C, Lilly J M, Early J J and Sykulski A M 2016 A global surface drifter data set at hourly resolution *J. Geophys. Res.: Oceans* **121** 2937–66

Essink S, Hormann V, Centurioni L R and Mahadevan A 2019 Can we detect submesoscale motions in drifter pair dispersion? *J. Phys. Oceanogr.* **49** 2237–54

Ferrari R and Wunsch C 2009 Ocean circulation kinetic energy: reservoirs, sources, and sinks *Annu. Rev. Fluid Mech.* **41** 253–82

Furuichi N, Hibiya T and Niwa Y 2008 Model-predicted distribution of wind-induced internal wave energy in the world's oceans *J. Geophys. Res.: Oceans* **113** C09034

Granata T, Wiggert J and Dickey T 1995 Trapped, near-inertial waves and enhanced chlorophyll distributions *J. Geophys. Res.: Oceans* **100** 20793–804

Hansen D V and Poulain P-M 1996 Quality control and interpolations of WOCE-TOGA drifter data *J. Atmos. Ocean. Technol.* **13** 900–9

Hersbach H *et al* 2020 The ERA5 global reanalysis *Q. J. R. Meteorol. Soc.* **146** 1999–2049

Jing Z, Wu L and Ma X 2017 Energy exchange between the mesoscale oceanic eddies and wind-forced near-inertial oscillations *J. Phys. Oceanogr.* **47** 721–33

Kunze E 1985 Near-inertial wave propagation in geostrophic shear *J. Phys. Oceanogr.* **15** 544–65

Laurindo L C, Mariano A J and Lumpkin R 2017 An improved near-surface velocity climatology for the global ocean from drifter observations *Deep-Sea Res.* I **124** 73–92

Liu G, Chen Z, Lu H, Liu Z, Zhang Q, He Q, He Y, Xu J, Gong Y and Cai S 2023 Energy transfer between mesoscale eddies and near-inertial waves from surface drifter observations *Geophys. Res. Lett.* **50** e2023GL104729

Liu Y, Jing Z and Wu L 2019 Wind power on oceanic near-inertial oscillations in the global ocean estimated from surface drifters *Geophys. Res. Lett.* **46** 2647–53

Lumpkin R and Johnson G C 2013 Global ocean surface velocities from drifters: mean, variance, El Niño–Southern Oscillation response, and seasonal cycle *J. Geophys. Res.: Oceans* **118** 2992–3006

Lumpkin R, Özgökmen T and Centurioni L 2017 Advances in the application of surface drifters *Annu. Rev. Mar. Sci.* **9** 59–81

Niiler P P and Paduan J D 1995 Wind-driven motions in the Northeast Pacific as measured by lagrangian drifters *J. Phys. Oceanogr.* **25** 2819–30

Oey L Y, Ezer T, Wang D P, Fan S J and Yin X Q 2006 Loop Current warming by Hurricane Wilma *Geophys. Res. Lett.* **33** L08613

Park J J, Kim K and King B A 2005 Global statistics of inertial motions *Geophys. Res. Lett.* **32** L14612

Pazan S E and Niiler P P 2001 Recovery of near-surface velocity from undrogued drifters *J. Atmos. Ocean. Technol.* **18** 476–89

Pollard R T 1970 On the generation by winds of inertial waves in the ocean *Deep-Sea Res.* **17** 795–812

Pollard R T and Millard R C 1970 Comparison between observed and simulated wind-generated inertial oscillations *Deep-Sea Res.* **17** 813–21

Poulain P-M 1990 Near-inertial and diurnal motions in the trajectories of mixed layer drifters *J. Mar. Res.* **48** 793–823

Price J F 1981 Upper ocean response to a hurricane *J. Phys. Oceanogr.* **11** 153–75

Qian Y-K, Peng S and Li Y 2013 Eulerian and lagrangian statistics in the South China sea as deduced from surface drifters *J. Phys. Oceanogr.* **43** 726–43

Röhrs J, Halsne T, Sutherland G, Dagestad K-F, Hole L R, Broström G and Christensen K H 2023 Current shear and turbulence during a near-inertial wave *Front. Mar. Sci.* **10** 1115986

Saha S *et al* 2014 The NCEP climate forecast system version 2 *J. Clim.* **27** 2185–208

Spydell M and Feddersen F 2009 Lagrangian drifter dispersion in the surf zone: directionally spread, normally incident waves *J. Phys. Oceanogr.* **39** 809–30

Thomson R E, LeBlond P H and Rabinovich A B 1998 Satellite-tracked drifter measurement of inertial and semidiurnal currents in the northeast Pacific *J. Geophys. Res.: Oceans* **103** 1039–52

Wang G, Wu L, Mei W and Xie S-P 2022 Ocean currents show global intensification of weak tropical cyclones *Nature* **611** 496–500

Wang T, Zhang S, Chen F, Ma Y, Jiang C and Yu J 2020 Influence of sequential tropical cyclones on phytoplankton blooms in the northwestern South China Sea *J. Oceanol. Limnol.* **39** 14–25

Wu W, Du Y, Qian Y K, Chen J and Jiang X 2022 Large South Equatorial current meander in the southeastern tropical indian ocean captured by surface drifters deployed in 2019 *Geophys. Res. Lett.* **49** e2021GL095124

Zhang S, Xie L, Hou Y, Zhao H, Qi Y and Yi X 2014 Tropical storm-induced turbulent mixing and chlorophyll-a enhancement in the continental shelf southeast of Hainan Island *J. Mar. Syst.* **129** 405–14

Zhang Z and Qiu B 2018 Evolution of submesoscale ageostrophic motions through the life cycle of oceanic mesoscale eddies *Geophys. Res. Lett.* **45** 11–847

Zhao Z, Wu W, Xia Y and Du Y 2023 Interior route and seasonal dynamics of the meridional current in the Eastern Indian ocean tropical gyre *J. Geophys. Res.: Oceans* **128** e2023JC019959